# Tectonic denudation and topographic development in the Spanish Sierra Nevada

L. J. Reinhardt,[1] T. J. Dempster,[2] J. F. Shroder Jr.,[3] and C. Persano[2]

Received 1 February 2006; revised 20 October 2006; accepted 8 December 2006; published 1 May 2007.

[1] The denudation history of the rapidly uplifting western part of the Spanish Sierra Nevada was assessed using apatite fission track (AFT) ages and $^{10}$Be analyses of bedrock and fluvial sediments. Major contrasts in the denudation history are recorded within the 27 km$^2$ Río Torrente catchment. Upland areas are characterized by low-relief, low slope angles, and locally the preservation of shallow marine sediments, which have experienced <200 m of erosion in the last 9 Myr. However, AFT age determinations from samples collected close to the marine sediments imply >2 km of denudation since circa 4 Ma. The minimum denudation rates of 0.4 mm yr$^{-1}$ derived from AFT also contrast with the slow medium-term ($10^4$ years) erosion rates (0.044 ± 0.015 mm yr$^{-1}$) estimated from $^{10}$Be measurements at high elevations. The local medium-long-term contrasts in denudation rates within the high Sierra Nevada indicate that much of the unroofing occurs by tectonic denudation on flat-lying detachments. In lower elevation parts of the catchment, rapid river incision coupled to rock uplift has produced ~1.6 km of relief, implying that the rivers and adjacent hillslopes close to the edge of the orogen are sensitive to normal-fault-driven changes in base level. However, these changes are not transmitted into the low-relief slowly eroding upland areas. Thus the core of the mountain range continues to increase in elevation until the limits of crustal strength are reached and denudation is initiated along planes of structural weakness. We propose that this form of tectonic denudation provides an effective limit to relief in young orogens. **Citation:** Reinhardt, L. J., T. J. Dempster, J. F. Shroder Jr., and C. Persano (2007), Tectonic denudation and topographic development in the Spanish Sierra Nevada, *Tectonics*, *26*, TC3001, doi:10.1029/2006TC001954.

## 1. Introduction

[2] Landsliding is the principal mode of denudation in tectonically active mountain belts [*Hovius et al.*, 1997]. This form of shallow gravitational collapse is often driven by high rates of river incision that force the hillslopes to maintain the threshold angle for landsliding [*Burbank et al.*, 1996], producing a landscape where mountain tops are lowered at the same rate as river incision. However, rock strength regulates the depth and frequency of bedrock landslides and the rate of landsliding may not be able keep pace with the rate of river incision, leading to the development of strength-limited relief [*Anhert*, 1970; *Schmidt and Montgomery*, 1995; *Roering et al.*, 2005]. In these situations, a variety of deeper level detachments may form and allow larger-scale gravitational collapse to occur within orogens [*Van Bemmelen*, 1954; *McClay et al.*, 1986; *Savage and Varnes*, 1987; *Mérnard and Molnar*, 1988; *Rey et al.*, 2001]. The exact nature of these deeper detachments remains ambiguous but involve exhumation of deeply buried crust by normal faulting [cf. *Ring et al.*, 1999] and are thought to range from "summit-lowering" landslides, termed sackung failure [*Dramis and Sorriso-Valvo*, 1994; *Shroder*, 1998; *Shroder and Bishop*, 1998], to deeper structures more traditionally thought of as responsible for tectonic denudation. Although tectonic denudation is widely recognized as an important orogenic process [*Chamberlain et al.*, 1991; *Hodges et al.*, 1992; *Hubbard et al.*, 1995; *Johnson et al.*, 1997; *Kuhleman et al.*, 2001; *Carrapa et al.*, 2003], it generally lacks an obvious surface expression. Consequently, the unroofing of rocks from beneath major detachments remains poorly constrained. Here we investigate the links between gravitational collapse via tectonic denudation and relief development in the Spanish Sierra Nevada, where an excellent record of denudation from 9 Ma to the present is preserved. The long-term (>$10^6$ years) pattern of denudation is assessed using a combination of apatite fission track (AFT) thermochronology and the stratigraphic record. Links between tectonic denudation and topographic development over $10^4$–$10^6$ year timescales are also investigated using cosmogenic $^{10}$Be erosion rate measurements.

## 2. Sierra Nevada

### 2.1. Geological Background

[3] The Spanish Sierra Nevada, a small 3500 m high mountain block, is part of the Betic Cordillera Internal zone, in the westernmost part of the Alpine orogen (Figure 1a). The Internal zone is composed of two relatively flat-lying

[1]Center for Earthquake Research and Information, University of Memphis, Memphis, Tennessee, USA.
[2]Department of Geographical and Earth Sciences, University of Glasgow, UK.
[3]Department of Geography and Geology, University of Nebraska at Omaha, Omaha, Nebraska, USA.


0278-7407/07/2006TC001954

metamorphic thrust sheets, the Alpujárride and Nevado-Filábride, separated by a major shear zone, the Betic Movement Zone (BMZ) [*Platt and Vissers*, 1989; *Johnson et al.*, 1997]. The BMZ dips at shallow angles away from the central core of the Sierra Nevada and contains mylonitized tourmaline granites, together with amphibolites, marbles and, locally metaevaporites. Tertiary sedimentary basins surround the Sierra Nevada (Figure 1a), and are

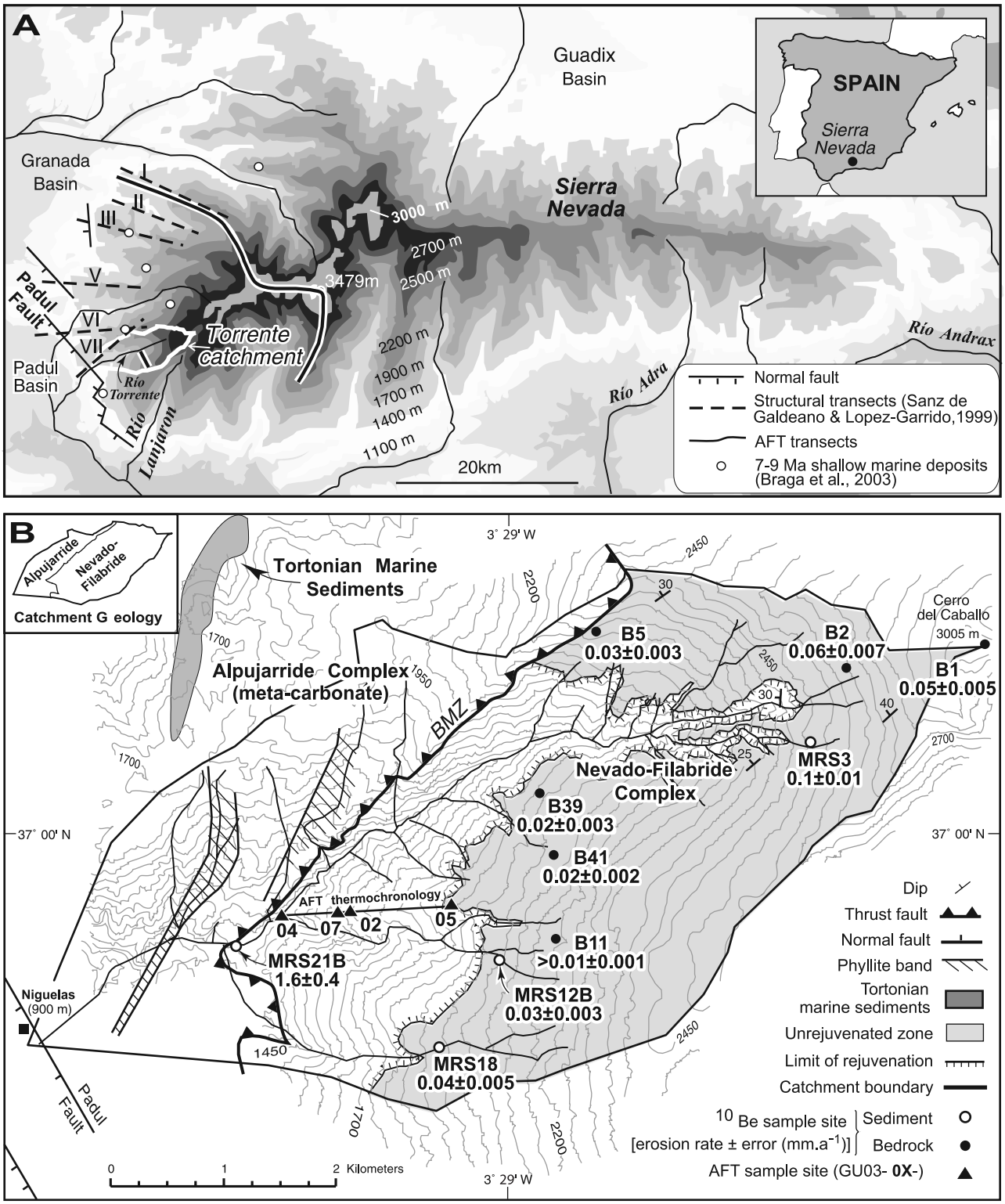


**Figure 1**

filled with coarse conglomerates derived from the uplifting mountain block [e.g., *Lonergan and Mange-Rajetzky*, 1994; *Calvache et al.*, 1997].

[4] The core of the elongated dome structure of the Sierra Nevada has been uplifted through a combination of low-angle extensional faulting and upright folding [*Martínez-Martínez et al.*, 2002; *Galindino-Zaldívar et al.*, 2003]. Scattered remnants of 7–9 Ma shallow marine deposits, preserved at elevations up to 1800 m, record the emergence of the Sierra Nevada as an island during the late Miocene [*Braga et al.*, 2003]. These coral reefs and coastal conglomerates are preserved on Alpujárride bedrock throughout the Sierra Nevada (Figure 1a), and their age broadly correlates with elevation, indicating that the highest topography emerged first. These deposits constrain mean surface uplift rates to 0.2 mm $yr^{-1}$ over the past 9 Myr for both eastern and western margins of the Sierra Nevada [*Braga et al.*, 2003]. In the context of the pattern of erosion in the Sierra Nevada, it is significant that these deposits were uplifted shortly after deposition and were <200 m thick [*Sanz de Galdeano and López-Garrido*, 1999; *Braga et al.*, 2003]. Their current maximum thickness of ~30 m on ridges in the high Sierra Nevada implies very low long-term surface erosion rates in some of the present interfluvial areas [*Sanz de Galdeano and López-Garrido*, 1999]. In contrast, high erosion rates are implied by the deposition of several extremely coarse Pliocene fan and braid deltas in the adjacent Granada basin [*Rodríguez-Fernández et al.*, 1989; *Hughes*, 1995]. These contrasting observations suggest that long-term denudation has been spatially variable.

[5] The Sierra Nevada metamorphic core was unroofed by tectonic denudation between 9 and 8 Ma exposing the underlying Nevado-Filábride complex [*Johnson*, 1997]. This core was strongly eroded between ~7 and 6.5 Ma, followed by a period of quiescence in the Messinian (~6 Ma). Other phases of increased subaerial erosion and/or the removal of overburden by tectonic processes [cf. *England and Molnar*, 1990] between 4 and 5 Ma are indicated by sedimentary evidence [*Fernández et al.*, 1996] and apatite fission track (AFT) ages, which are younger in the highest elevation parts of the belt (Figure 2) [*Johnson*, 1997]. The close proximity of rocks containing young 4–5 Ma AFT ages [*Johnson*, 1997] and the >7 Ma marine sediments also points to spatial variability in long-term denudation.

[6] The topography of the Sierra Nevada is characterized by rounded mountain tops and deep valleys. Our analysis indicates that valley incision has resulted in a mean relief of 1640 ± 600 m in the western Sierra Nevada (n = 27 catchments), while above 2000 m summit areas have low-angle hillslopes (mean = 13°) that are well below threshold angles for landsliding. Quaternary glaciation was restricted to valley glaciers and had little effect on upland morphology. Moraines throughout the western and northern Sierra record four cold episodes of decreasing ice extent during the last two glacial periods (~200–130 ka and 80–10 ka). During the Last Glacial Maximum, valley glaciers extended down to 2625 m [*Lhénaff*, 1977; *Sánchez et al.*, 1990; *Simón et al.*, 2000; *Gómez-Ortiz et al.*, 1996]. Modern periglacial activity is only seen at altitudes above 3000 m [*Simón et al.*, 2000; *Gómez et al.*, 2001] and is unlikely to be important in the study area, which has a maximum elevation of 3005 m.

### 2.2. Torrente Catchment

[7] The Río Torrente occupies a 27 $km^2$, 2-km-relief semiarid catchment in the western Sierra Nevada (Figure 1b). The BMZ divides the catchment into two lithological sectors along a NE-SW axis. The Alpujárride complex NW of this axis is composed of a thick (>2 km) succession of NW dipping low-grade dolomitic marbles with occasional thin (~10 m) units of phyllite. The latter have a strong deformation fabric suggesting that they may have accommodated movements between more massive dolomitic units and slickensided surfaces are also common in these dolomitic units. These dolomites are highly brecciated in a broad 1 km zone at the mountain front [*Calvache et al.*, 1997]. The structurally lower Nevado-Filábride unit, which is the focus of our analytical work, lies to the SE of the BMZ and is dominated by graphitic schist with ubiquitous quartz veins. The Torrente catchment comprises two geomorphic zones (Figure 1b) separated by an upstream migrating knickzone (Figure 3) [cf. *Whipple and Tucker*, 1999]. The upper, headwater parts of the catchment have low slope angles (<25°), a thin regolith cover with dense low-lying vegetation and low rates of fluvial incision [*Sánchez-Marañón et al.*, 1996]. The lower catchment is steeper (slope angles of 25° to 90°), sparsely vegetated and erosive processes are dominated by shallow bedrock landslides (Figure 4). The depth of landsliding is limited by the strong schistosity of the Nevado-Filábride portion of the lower catchment and no landslide head scarps >1 m in depth are observed.

[8] The exit to the catchment coincides with the Padul Fault, which is part of a major fault array that marks the SW edge of the Sierra Nevada (Figure 1a). Late Pleistocene to Holocene movement of this fault has resulted in the development of a 50 m high scarp at the catchment exit [*Calvache et al.*, 1997; *Sanz de Galdeano*, 1996; *Alfaro et*

**Figure 1.** Topographic, geological, and geomorphic maps of the Sierra Nevada and Río Torrente catchment. (a) Topographic map of the Sierra Nevada generated from 30 arc sec GTOPO30 digital elevation data. The locations of the following are shown: the Tortonian marine sediments overlying Alpujárride bedrock [*Braga et al.*, 2003]; the AFT sample profiles in the central and western Sierra Nevada; the normal fault zone in the western Sierra Nevada; and the structural sections constructed by *Sanz de Galdeano and López-Garrido* [1999], as shown in Figure 6. (b) Geological and geomorphic map of the Río Torrente catchment. The topographic data were generated from a 3 m digital elevation model. The locations of the following are shown: cosmogenic nuclide samples and the erosion rates estimated from the $^{10}Be$ concentrations of these samples; AFT sample sites (see also Figure 2), and the Tortonian marine sediments adjacent to the catchment.

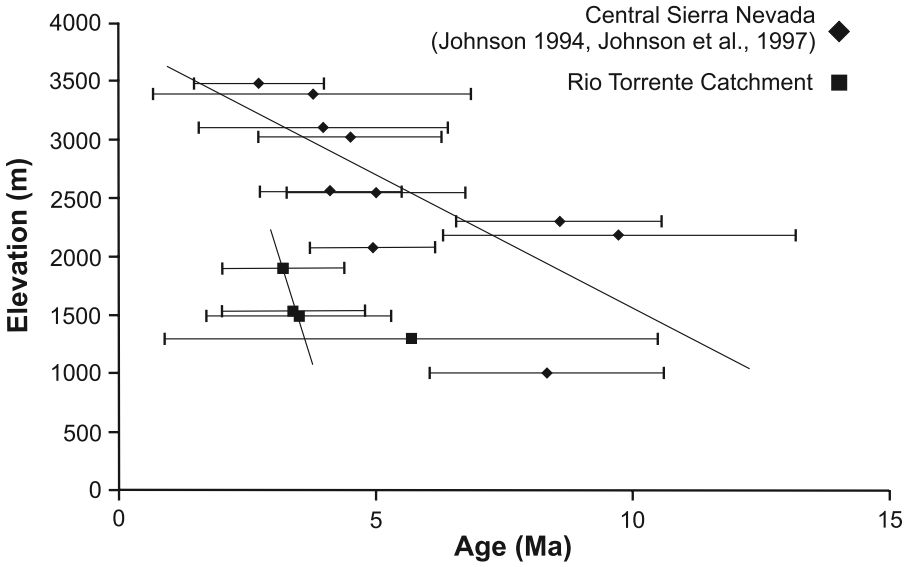


**Figure. 2.** Apatite fission track pooled ages versus elevation from the Torrente catchment. AFT measurements from the central Sierra Nevada are also plotted [*Johnson*, 1994; *Johnson et al.*, 1997]. All error bars are $2\sigma$.

*al.*, 1999; *Reinhardt*, 2005]. The normal fault array is also linked to 420 m of vertical displacement in the Pleistocene alluvial fan sediments of the Alhambra Formation, 10 km NW of the Torrente catchment since 0.5–1 Ma [*Sanz de Galdeano*, 1996; *Keller et al.*, 1996; *Sanz de Galdeano and López-Garrido*, 1999]. This observation implies a relative rock uplift rate of at least 0.4–0.8 mm $yr^{-1}$ in the last 1 Myr. In addition, the Río Andarax, a 1200 $km^2$ catchment river located 70 km east of the Torrente (Figure 1a), has incised at a rate approximating rock uplift over the past 250 kyr (0.3–0.7 mm $yr^{-1}$ [*García et al.*, 2003]). The similar estimates of rock uplift rates (in the sense of *England and Molnar* [1990]) from widely separated parts of the orogen, combined with the simple structure of the Sierra Nevada [*Martínez-Martínez et al.*, 2002; *Galindino-Zaldívar et al.*, 2003], is taken to indicate that the Torrente catchment and the rest of the Sierra Nevada has been uplifting relative to the footwall block at ~0.5 mm $yr^{-1}$ since the middle to late Pleistocene. This is consistent with the pattern of uniform post-9 Ma surface uplift inferred from the Tortonian marine sediments that uplifted with the Sierra Nevada (Figure 1a) [*Braga et al.*, 2003].

## 3. Methods

[9] We used a range of methods to constrain topographic development and denudation in the Sierra Nevada over a variety of timescales. These include apatite fission track (AFT) thermochronology which records the exhumation of material as it passes through a depth range of 2–5 km enabling measurement of mean denudation rates over million year timescales [*Gleadow and Brown*, 2000] and $^{10}$Be analysis which can measure subaerial erosion rates over $10^2$–$10^5$ year timescales [*Lal*, 1991; *Brown et al.*, 1995; *Bierman and Steig*, 1996; *Granger et al.*, 1996].

### 3.1. Cosmogenic $^{10}$Be Measurements

[10] We analyzed $^{10}$Be in bedrock samples and quartz grains in modern fluvial sediments. Six bedrock samples were collected from exposures in the slowly eroding upper catchment (Figure 1b). For each bedrock sampling site, 3–10 individual samples of vein quartz were crushed and amalgamated from up to three widely spaced outcrops (up to 100 m apart) at the same altitude [*Reinhardt et al.*, 2007]. Modern fluvial sediments were collected from four river reaches, three in the upper and one in the lower catchment (Figure 1b). At sediment-sampling sites ~5 kg of 0.25–0.5 mm sized clasts were collected from the surface layer (<0.2 m depth) along a 10 m reach of the river. In order to interpret $^{10}$Be concentrations in fluvial sediments in terms of mean upstream erosion rates [*Brown et al.*, 1995;

**Figure 3.** Northeasterly looking view of the upper Torrente catchment. The inflection in hillslope and channel at the head of the knickzone is highlighted with a white dotted line.

**Figure 4.** Downstream view of the middle, rejuvenated reaches of the Río Torrente. The hillslopes are dominated by shallow bedrock landsliding.

*Bierman and Steig*, 1996; *Granger et al.*, 1996], we generated a 3 m resolution DEM from 1:20 000 aerial photographs of the Torrente catchment and calculated the $^{10}$Be production rate for each cell [*Granger and Smith*, 2000; *Granger et al.*, 2001; *Stone*, 2000; *Codilean*, 2006].

[11] The $^{10}$Be content of bedrock outcrops and fluvial sediments were measured from quartz extracted using preparation methods similar to those described by *Bierman et al.* [2002]. All quartz grains for $^{10}$Be analysis were treated with 30% HCl and passed though a Frantz magnetic separator. During magnetic separation many ''impure'' quartz grains were directed into the nonquartz fraction resulting in an underestimation of the quartz content of each sample. However, this systematic error applies equally to all sediment samples derived from the same lithology (schist) and a direct comparison between the quartz content of each magnetically separated sediment sample is therefore reasonable. The estimated quartz content of the sediment samples is 11 ± 2% [*Reinhardt*, 2005] indicating that the quartz content of source area bedrock is approximately uniform. The nonmagnetic fraction of each sample was lightly crushed and ultrasonically etched (repeatedly, if necessary) in 2% HF/2% $HNO_3$ to isolate pure quartz, with Al <100 ppm as measured by atomic absorption spectroscopy [*Kohl and Nishiizumi*, 1992]. A 250 $\mu$g spike of $^{9}$Be was added to each pure quartz sample and the $^{10}$Be/$^{9}$Be ratio measured by AMS at the Department of Nuclear Physics, Australian National University, Canberra [*Fifield*, 1999]; a 3% AMS measurement error is incorporated into all calculations.

### 3.2. Apatite Fission Track Thermochronology

[12] We collected four AFT samples from the Torrente catchment in order to link a local estimate of long-term denudation to both the structures within the immediate area and the wider pattern of AFT-based denudation in the orogen [*Johnson et al.*, 1997]. Samples of 3–4 kg bedrock schist from the Nevado-Filábride complex were taken along a vertical profile from 1295 to 1900 m elevation, perpendicular to the BMZ on the south side of the Río Torrente (Figure 1b). The 64–355 $\mu$m fraction was separated by crushing and sieving, and standard techniques of heavy liquid and magnetic separation were used to obtain apatite concentrates with a purity of about 80%. AFT analyses were performed using the external detector method and zeta calibration approach, using 0.5 as the geometry correction factor [*Hurford and Green*, 1982]. Apatite grains were etched for 22 s with a 5 M nitric acid at room temperature (~20°C). The muscovite external detectors were etched for 28 min using 48% hydrofluoric acid. The samples were irradiated at the High Flux Australian Reactor (HIFAR) in Sydney and the constancy of the neutron flux was checked using the CN5 uranium glass dosimeter. Spontaneous and induced tracks were counted using a Zeiss axioplan microscope with a ×100 dry objective and a total magnification of ×1600. No confined horizontal track lengths were observed.

## 4. Results

### 4.1. Apatite Fission Track: Long-Term Denudation of the Sierra Nevada (>$10^6$ years)

[13] Central apatite fission track ages range between 5.7 ± 4.8 Ma (GU03-04) and 3.2 ± 1.2 Ma (GU03-05) with between 42% and 87% of the counted grains in each sample yielding zero fission track ages (Table 1): errors are cited ±2$\sigma$. The ages of the single grains where tracks were visible vary up to a maximum of ~30 Ma (GU03-04); two grains yielding fission track ages of 29 and 32 Ma were analyzed. Similarly, old fission track grain ages from samples close to the BMZ have been reported by *Johnson* [1997], and they may represent an inherited component and hence lower grades of late Alpine metamorphism at higher structural levels. For this reason the 5.7 Ma sample (GU03-04) is not considered in our analysis. Further, the lack of confined horizontal track lengths makes any detailed thermal modeling impossible.

[14] The AFT thermochronometer provides information on a rock's thermal history below ~110°C. The predominance of grains with no tracks indicate that these samples have been recently and rapidly exhumed from depth of ~110°C. A rapid exhumation is also corroborated by the uniformity of AFT sample ages collected over a vertical distance of ~600 m (Figure 2). The presence of zero-age grains and the values of the central ages suggest that a rapid cooling occurred during the past 3–4 Myr; postdating the ductile movements on the BMZ [*Johnson et al.*, 1997; *Johnson*, 1997]. We estimate that the average rate of cooling of samples from 110°C to the surface, taking into account the 2$\sigma$ uncertainties on the individual ages (excluding sample GU03-04), ranges between 21 and 65°C Myr$^{-1}$. Converting these cooling rates to denudation rates requires an estimation of the geothermal gradient present during exhumation. Geothermal gradients in orogens are poorly known and can vary considerably within the shallow crust, especially within highly fractured rocks [*Dempster and*

**Table 1.** Apatite Fission Track Data From the Río Torrente Catchment[a]

| Sample | Longitude (WGS84) | Latitude (WGS84) | Elevation, m | Number of Crystals | Spontaneous $\rho_s$ ($N_s$) | Induced $\rho_i$ ($N_i$) | $P\chi^2$, % | Dosimeter $\rho_\Delta$ ($\delta N$) | Central FT Age, Ma | Uranium Concentration, ppm |
|---|---|---|---|---|---|---|---|---|---|---|
| GU03-05 | 3°29′30″ W | 36°59′31″ N | 1900 | 31 | 0.139 (28) | 5.286 (1067) | 51.78 | 6.53 (5739) | 3.2 ± 1.2 | 9 |
| GU03-02 | 3°30′07″ W | 36°59′29″ N | 1530 | 50 | 0.064 (22) | 2.111 (722) | 100 | 6.06 (5739) | 3.4 ± 1.4 | 4 |
| GU03-07 | 3°30′10″ W | 36°59′29″ N | 1492 | 28 | 0.087 (17) | 2.952 (580) | 96.65 | 6.4 (5739) | 3.5 ± 1.8 | 6 |
| GU03-04 | 3°30′32″ W | 36°59′28″ N | 1295 | 31 | 0.028 (6) | 0.547 (119) | 82.77 | 6.198 (5739) | 5.7 ± 4.8 | 2 |

[a]Counting measurements were carried out by C. Persano ($\xi = 368 \pm 8$, dosimeter CN5). Dosimeter track densities $\rho_D$, spontaneous ($\rho_S$) and induced ($\rho_I$) track densities are in $10^5$ tr cm$^{-2}$. The fission track ages were calculated using Trackkey [*Dunkl*, 2002] and are reported with a $2\sigma$ error. Uranium concentrations are also reported to highlight the fact that uncertainties in the AFT ages are strongly dependent of the abundance of U in the single apatite crystals.

*Persano*, 2006]. However, we do have evidence that the geothermal gradient in the Sierra Nevada was unusually high. The stability of late andalusite throughout much of this region [*Argles et al.*, 1999] suggests a geothermal gradient of ~50°C km$^{-1}$ at circa 20 Ma. This gradient is likely to have relaxed after the metamorphic peak and so we assume 50°C km$^{-1}$ as a maximum value. This estimate suggests that denudation rates over the last 3–4 Myr ranges between 1.5 and 0.4 mm yr$^{-1}$, implying ~2 km denudation. Using a lower assumed value for the geothermal gradient (30°C km$^{-1}$ [*Johnson*, 1997]) suggests an averaged denudation rate of 1.4 mm yr$^{-1}$ similar to the 1.2 mm yr$^{-1}$ value of *Johnson* [1997] and implying ~3.5 km of denudation. Thus between 2 km and 3.5 km of crust has been denuded over the past 3–4 Myr, at a rate of unroofing similar to that determined by AFT thermochronology in other active orogens [*Hurford et al.*, 1989; *Sorkhabi et al.*, 1996].

[15] The lack of track length measurements prevents the possibility of better constraining the timing and duration of this denudational event. Qualitatively the predominance in almost all the samples of grains with zero age suggests that this event may be even more recent than 3–4 Ma, but the uncertainty in our AFT age estimates prohibits such speculation. Instead, we note that both our AFT data and that of *Johnson* [1997] are consistent with the phase of increased erosion and sedimentation between 4 and 5 Ma reported by *Fernández et al.* [1996].

### 4.2. Cosmogenic $^{10}$Be Measurements: Denudation in the SW Sierra Nevada Over the Past $10^2$–$10^5$ years

[16] Measurement of $^{10}$Be concentrations in bedrock and fluvial sediments may provide steady state erosion rate estimates over $10^2$–$10^5$ year timescales [*Lal*, 1991; *Bierman and Steig*, 1996; *Granger et al.*, 1996]. This method is therefore capable of linking short-medium term patterns of erosion both to the development of relief and present-day geomorphological processes. We have used one of the best constrained cosmogenic nuclide systems, $^{10}$Be in quartz [*Gosse and Phillips*, 2001], to assess the pattern and rate of erosion in the Río Torrente catchment (Figure 1b). The interpretation of $^{10}$Be concentrations in bedrock and fluvial sediment samples in terms of steady state erosion rate is subject to a number of complicating factors [*Lal*, 1991; *Bierman and Steig*, 1996; *Granger et al.*, 1996; *Small et al.*, 1997; *Gosse and Phillips*, 2001; *Vance et al.*, 2003] that are discussed in Appendix A. However, we stress that the order-of-magnitude differences in erosion rates reported here are highly robust.

[17] Estimates of $^{10}$Be based erosion rates in the Torrente catchment reveal a 2 order-of-magnitude variation (Tables 2a and 2b and Figure 1b), reflecting the contrasting geomorphic processes associated with ongoing rejuvenation. The $^{10}$Be concentration within fluvial sediments (MRS 21B) collected in the lower landslide-dominated catchment (Figure 4) yield a high erosion rate of 1.6 ± 0.4 mm yr$^{-1}$. This short-term ($10^2$ years) erosion rate is an order of magnitude greater than the long-term ($10^5$ years) rate of relative rock uplift (~0.5 mm yr$^{-1}$), suggesting considerable variation in short-term fluvial incision rates: the rock uplift rate was estimated from vertical displacement of alluvial fan sediments and equilibrium river incision. Conversely, erosion in the unrejuvenated upper catchment is 1 order of magnitude lower than the long-term rate of rock uplift (see Figure 1b and Tables 2a and 2b). Both bedrock outcrops (0.036 ± 0.01 mm yr$^{-1}$, n = 5) and soil-mantled slopes (0.057 ± 0.012 mm yr$^{-1}$, n = 3) are eroding at uniformly low rates over the characteristic timescale of 12 ka (i.e., the time required to erode 0.6 m, when $^{10}$Be accumulation is most sensitive to surface erosion [*Bierman and Steig*, 1996]).

## 5. Denudation History of the Western Sierra Nevada

[18] The denudation history of the western Sierra Nevada is characterized by marked contrasts between the rate of erosion in river valleys and low-relief upland areas (Figure 5). The concordance between in situ bedrock and mean catchment-scale $^{10}$Be-derived erosion rates in the upland portion of the Torrente catchment implies that the rates of river incision and hillslope lowering are approximately equal, with a mean upland erosion rate of 0.044 ± 0.015 mm yr$^{-1}$ (n = 8). This similarity points to a mature drainage network in the upland part of the western Sierra Nevada [cf. *Hovius et al.*, 1998], where slow diffusive processes dominate hillslope erosion. Further, the continued presence of marine rocks on Alpujárride basement at high elevations indicates that this low medium-term ($10^4$ years)

**Table 2a.** Bedrock Erosion Rates[a]

| | Longitude (WGS84) | Latitude (WGS84) | Altitude, m | $^{10}$Be Production Rate, Clear 2$\pi$ Horizon, atoms g$^{-1}$ yr$^{-1}$ | Thickness Correction Factor | Shielding Correction Factor | $^{10}$Be Concentration, $10^3$ atoms g$^{-1}$ $SiO_2$ | Bedrock Erosion Rate, mm yr$^{-1}$ |
|---|---|---|---|---|---|---|---|---|
| B 1 | 3°26′23″ W | 37°00′43″ N | 3005 | 41.0 ± 4.2 | 0.98 ± 0.01 | n/a | 486 ± 14 | 0.05 ± 0.005 |
| B 2 | 3°27′13″ W | 37°00′37″ N | 2540 | 30.8 ± 3.1 | 0.98 ± 0.01 | 0.99 ± 0.05 | 329 ± 20 | 0.06 ± 0.007 |
| B 5 | 3°28′41″ W | 37°00′46″ N | 2170 | 24.2 ± 2.5 | 0.97 ± 0.01 | 0.97 ± 0.08 | 557 ± 27 | 0.03 ± 0.003 |
| B 11 | 3°28′51″ W | 36°59′21″ N | 2130 | 23.5 ± 2.4 | 0.99 ± 0.01 | n/a | 1635 ± 60 | >0.01 ± 0.001[b] |
| B39 | 3°29′01″ W | 37°00′01″ N | 1910 | 20.3 ± 2.1 | 0.98 ± 0.06 | 0.76 ± 0.07 | 414 ± 18 | 0.02 ± 0.003 |
| B 41 | 3°28′50″ W | 36°59′43″ N | 2030 | 22.0 ± 2.2 | 0.97 ± 004 | 0.75 ± 0.02 | 475 ± 24 | 0.02 ± 0.002 |

[a]The $^{10}$Be production rate (muon and spallation) at sea level and high latitude (5.1 ± 0.3 atom g$^{-1}$ yr$^{-1}$) is scaled to the appropriate latitude and altitude using the scaling parameters of *Stone* [2000]. Cited in situ bedrock $^{10}$Be production rates are not corrected for sample thickness or exposure geometry, but the necessary correction factors are listed. These $^{10}$Be production rate thickness and shielding correction factors use an attenuation length of 160 g cm$^{-2}$ and rock density of 2.71 g cm$^{-3}$ [*Dunne et al.*, 1999]. Catchment wide $^{10}$Be production rates are calculated from a 3 m digital elevation model and corrected for topographic shielding [*Codilean*, 2006] using the mean of all upstream cells. The erosion rate formulations of *Granger and Smith* [2000] and *Granger et al.* [2001, equation 1] are used to calculate mean catchment and bedrock erosion rates from (1) the $^{10}$Be concentration of (0.25–0.5 mm) fluvial quartz, collected from sandbars along a 20–30 m reach: 4 g of pure quartz was isolated for MRS18 and between 45 and 56 g for the other three sediment samples and (2) multiple quartz veins collected from one or more closely spaced bedrock exposures: bedrock sample thicknesses in centimeters are as follows: B1(2.1), B2(2.2), B5(2.3), B11(1.4), B39(2.8), B41(3.2). Uncertainties represent one standard error measurement uncertainty; production rate, and other errors [*Gosse and Phillips*, 2001] are fully propagated and added in quadrature; n/a, not applicable.

[b]The erosion rate calculated from sample B11 (>0.01 ± 0.001) must be interpreted as a minimum value because the sample had a cosmic ray exposure geometry >2$\pi$ [*Dunne et al.*, 1999].

erosion rate is representative of the long-term (>1 Myr) rate of erosion at high altitudes. Thus there is a significant disequilibrium between surface erosion rates over the past $10^4$ years to $10^6$ years (~0.04 mm yr$^{-1}$) at high altitudes and the estimated rate of regional rock uplift (~0.5 mm yr$^{-1}$). The order-of-magnitude difference between these two rates indicates that surface processes acting on these upland surfaces are unable to keep pace with rock uplift. It follows that the mountain range is not in topographic steady state and upland areas continue to increase in elevation. In contrast, over similar timescales the valleys of the western Sierra Nevada have developed ~1.6 km of relief, indicating that fluvial incision is locally efficient and capable of transporting material at a rate approximating to that of rock uplift over long timescales. Hence rapid rock uplift must inevitably lead to increased relief of the mountain range, which develops with steep valley sides and a relatively flat top.

[19] Our AFT age determinations from high-elevation parts of the Torrente catchment imply that at least 2 km of denudation has occurred in the past ~4 Myr, in agreement with other thermochronological determinations from the Nevado-Filábride bedrock [*Johnson*, 1997; *Johnson et al.*, 1997]. These latter studies identified a major phase of tectonic denudation that occurred on the BMZ between 9 and 8 Ma and in addition reported a general decrease in AFT ages toward high-elevation areas similar to the relationships we observe in the Torrente catchment (Figure 2). These age-elevation trends imply that denudation has been preferentially focused near the mountain tops and must either be linked to a period of accelerated surface erosion in the central Sierra Nevada at 4–5 Ma [*Johnson*, 1997; *Johnson et al.*, 1997] or another period of tectonic denudation affecting the core of the orogen. Importantly, the preservation of Tortonian sedimentary rocks on high-elevation Alpujárride basement rocks (Figures 1a and 5) dictates that the rate of surface erosion has remained exceptionally low in some upland areas over the past 9 Myr [*Sanz de Galdeano and López-Garrido*, 1999; *Braga et al.*, 2003]. Hence surface erosion cannot be responsible for the >2 km of denudation implied by the youngest AFT determinations, as such a scale of erosional unroofing must have affected all upland areas including those areas where

**Table 2b.** Mean Erosion Rates Calculated From 0.25–0.5 mm Sized Sediment[a]

| | Longitude (WGS84) | Latitude (WGS84) | Altitude Range, m | Mean $^{10}$Be Production Rate, atoms g$^{-1}$ yr$^{-1}$ | $^{10}$Be Concentration, $10^3$ atoms g$^{-1}$ $SiO_2$ | Mean Catchment Erosion Rate, mm yr$^{-1}$ |
|---|---|---|---|---|---|---|
| *Unrejuvenated Upper Catchment* | | | | | | |
| MRS 3 | 3°27′25″ W | 37°00′15″ N | 2470–2750 | 32.3 ± 3.2 | 211 ± 11 | 0.1 ± 0.01 |
| MRS 12B | 3°29′15″ W | 36°59′14″ N | 1970–2520 | 26.2 ± 2.6 | 650 ± 25 | 0.03 ± 0.003 |
| MRS 18 | 3°29′37″ W | 36°58′51″ N | 1900–2470 | 23.5 ± 2.3 | 397 ± 45 | 0.04 ± 0.005 |
| *Rejuvenated Lower Catchment* | | | | | | |
| MRS 21B | 3°30′46″ W | 36°59′20″ N | 1150–3005 | 23.7 ± 2.4 | 10.5 ± 2.7 | 1.6 ± 0.4 |

[a]See Table 2a footnote.

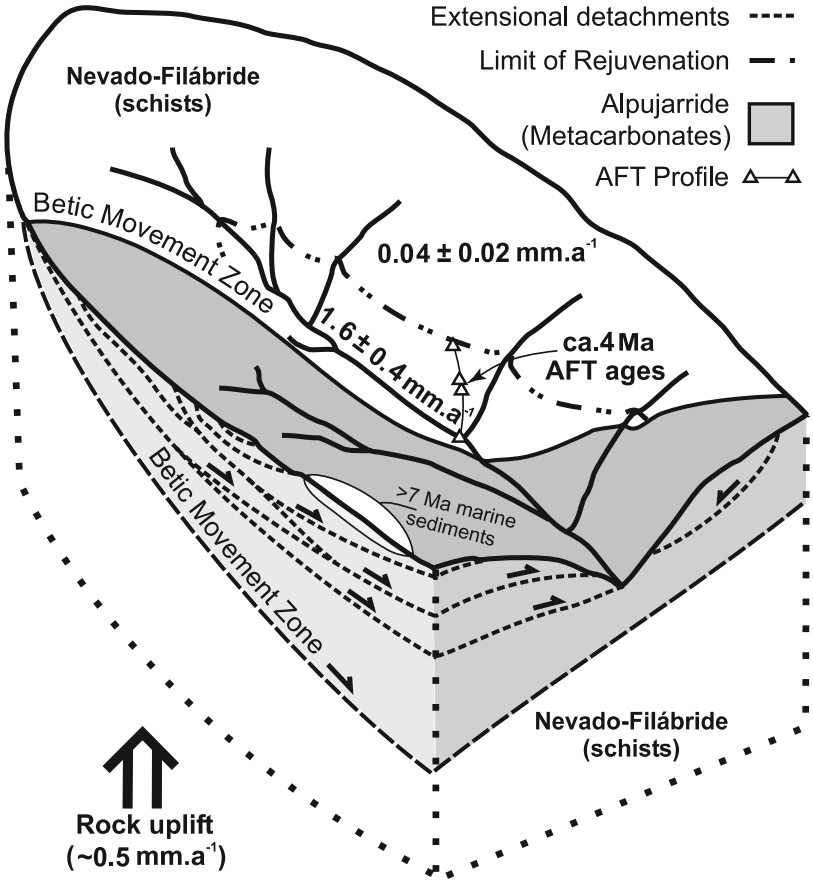


**Figure 5.** Block model of the Torrente catchment showing idealized geological structure. This model emphasizes the spatial relationship between circa 4 Ma AFT age estimates implying >2 km of denudation, >7 Ma marine sediments implying <200 m of denudation and the 2 order-of-magnitude difference between $^{10}$Be surface erosion rate estimates in rejuvenated and unrejuvenated areas.

marine sediments are observed today. The abrupt contrast in denudation implied by the proximity of young AFT ages and the remnants of old marine sediments can only be explained by fault-controlled exhumation and so the localized rapid denudation of upland areas since circa 4 Ma must involve unroofing via extensional detachments above the Nevado-Filábride core. This process of tectonic denudation, promoted by rapid surface uplift coupled with inefficient upland erosion, could potentially remove significant volumes of crust from high-elevation footwall areas without significant subaerial erosive denudation of the high-elevation hanging wall rocks. The movement of these blocks away from the central uplands on extensional detachments during the past ~4 Myr could account for relatively young AFT ages within the central core areas and generate the apparent negative age-elevation relationship observed by *Johnson* [1997] in the western Sierra Nevada (Figure 2). Tectonic denudation at this time must also have influenced topography and surface processes and may have been responsible for the pulse of clastic sediments in the Granada basin [*Fernández et al.*, 1996]. The general geomorphic signature associated with tectonic denudation seems likely to be steep-sided, flat-topped mountain ranges.

[20] The reactivation of the BMZ is one obvious candidate for a tectonic denudation [*Platt and Behrmann*, 1986]. However, the early structural fabrics within the mylonites form at significantly higher temperatures than those required by the cooling of the AFT system [*Gallagher*, 1995]. *Sanz de Galdeano and López-Garrido* [1999] have identified several low-angle extensional detachments within the Alpujárride complex of the western Sierra Nevada (Figures 1a and 6). These extend to depths of ~1.5 km, and typically terminate along the western mountain front against active normal faults. The geometry of these brittle extensional structures is consistent with these detachments being driven by surface uplift of the Sierra Nevada (Figure 5) [*Sanz de Galdeano and López-Garrido*, 1999], sufficient to cause gravity sliding along the shallowly dipping structures and weak phyllites and schists of the Alpujárride and Nevado-Filábride units. Thus the brecciation of Alpujárride dolomites close to the mountain front is probably due to the toe of the detachments continually overstepping the bounding faults (Figure 7), as envisaged by *Beck* [1968]. No large fault scarps associated with such detachments are obvious in the high Sierras, but slickensided surfaces are common in Alpujárride bedrock. The absence of

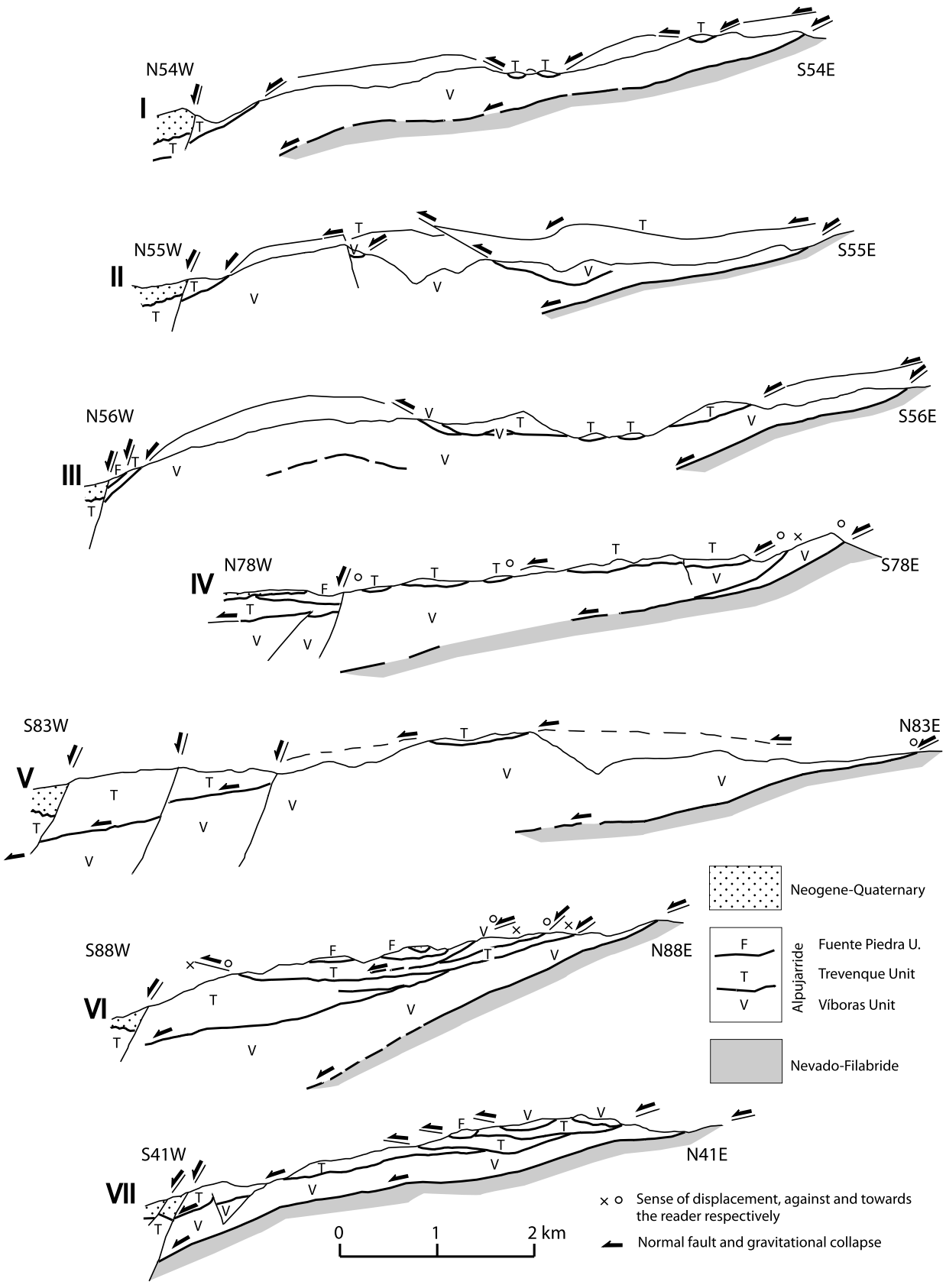


**Figure 6.** Structural cross sections through Alpujárride bedrock in the western Sierra Nevada [from *Sanz de Galdeano and López-Garrido*, 1999]. The location of each cross section is shown in Figure 1a.

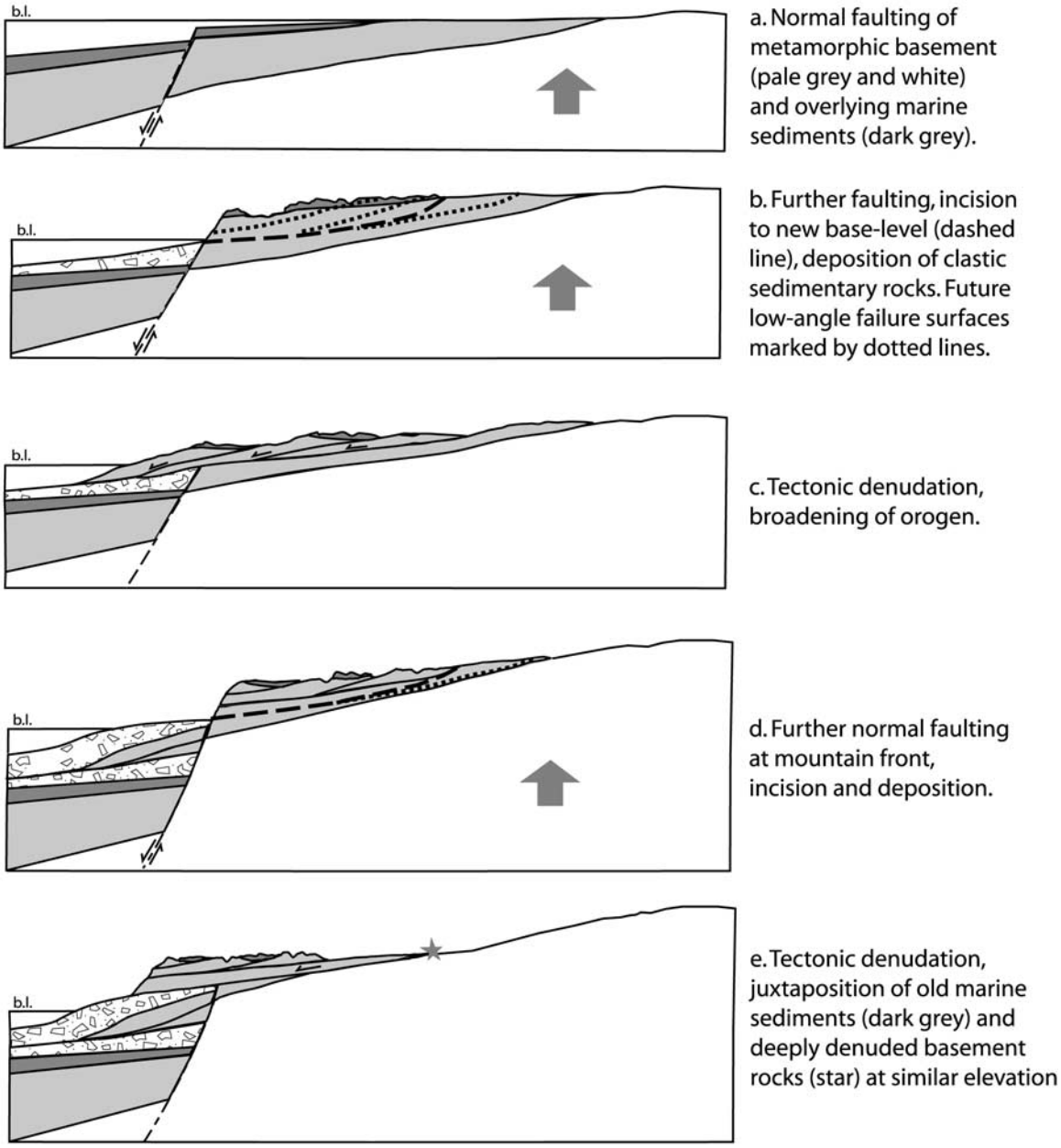


**Figure 7.** Cartoons showing the development of tectonic denudation in response to rock uplift, basement faulting, base level change, and fluvial incision. Normal faulting at the edge of the orogen progressively generates relief and brecciates rocks at the mountain front, while periodic tectonic denudation broadens the orogen and unroofs the core.

fault scarps may be a reflection of the generally flat-lying nature of the structures within the orogen and so the detachments tend not to produce steeply dipping scarp faces.

## 6. A Model for the Topographic Development of Young Orogens

[21] The denudation record of the Sierra Nevada over the past ~4 Myr is consistent with unroofing having been accomplished by two different mechanisms, subaerial erosion at the edge of the orogen and tectonic denudation of the core (see summary in Figure 8). We suggest that these two mechanisms are linked and that in response to rapid uplift, inefficient river incision promotes relief generation until the limits of crustal strength are reached, whereupon gravity sliding is initiated along structural weaknesses (Figure 7). In this model tectonic denudation occurs episodically (Figures 7c and 7e) in response to the attainment of critical

| Evidence | Interpretation | Conclusion |
|---|---|---|
| **Boundary of mountain block**<br>Significant recent vertical movement on Padul fault (1,2,3,4) | **Increasing elevation of summits**<br>Rapid rock uplift over the past $10^3$ – $10^6$ years | ***Rapid tectonic denudation driven by increasing relief of mountain belt due to inefficient fluvial incision at high elevations*** |
| **Valleys**<br>*(Geomorphology & Cosmogenic isotopes)*<br>Deep valleys (~1.5 km)<br>Low $^{10}$Be concentration in sediment | **Rapid river incision**<br>Efficient, long (>$10^5$ a) term river incision<br>Rapid incision and hillslope erosion over short term (>1 mm.a$^{-1}$) | |
| **Uplands**<br>*(Geology, Cosmogenic isotopes & Geomorphology)*<br>Local preservation of >7 Ma marine sediments (5)<br>High $^{10}$Be concentrations in sediment and bedrock<br>Low angle, low relief hillslopes | **Slow erosion**<br>Locally ca. 200 m of erosion over long term<br>Slow erosion over medium term (0.044 mm.a$^{-1}$)<br>Slow diffusive processes dominate erosion | |
| **Thermochronology**<br>Young AFT ages in core of orogen, older in peripheral areas (6) | **Locally rapid denudation**<br>ca. 2 km of denudation in past 3-4 Ma, focused in the core of the orogen | |
| **Structures**<br>Strong deformation fabric in phyllites and slickensided surfaces<br>Extensional detachments in cross-section (4)<br>Brecciation at mountain front (7) | **Fault controlled denudation**<br>Presence of tectonic detachments up to 1.5 km depth | |

**Source of data**: (1) Reinhardt, 2005; (2) Sanz de Galdeano, 1996; (3) Keller et al., 1996; (4) Sanz de Galdeano & López Garrido, 1999; (5) Braga et al., 2003; (6) Johnson, 1994; (7) Calvache et al., 1997.

**Figure 8.** Summary table of denudation history of the western Sierra Nevada.

shear values associated with the continued production of relief (Figures 7a, 7b, and 7d).

[22] The relationship between relief generation and tectonic denudation seems unlikely to be unique to the Sierra Nevada. Other mountain belts, such as the Himalaya and New Zealand Alps, show a suite of features linked to gravitational collapse ranging from orogen-scale normal faults to sackung collapse of ridges and individual slope failures [*Beck*, 1968; *Shroder and Bishop*, 1998]. The larger of these are thought to pass into ductile zones at depth [*Kapp and Guynn*, 2004; *Edwards and Harrison*, 1997; *Garzione et al.*, 2003], whereas the sackung and smaller brittle failure surfaces may become listric faults that intersect the surface on lower slopes of the orogen [cf. *Beck*, 1968]. We propose that the process of tectonic denudation of high-relief orogens should incorporate all scales of brittle detachments as they represent a continuum and are all controlled by a combination of high relief and unstable detachment surfaces. We suggest that deformation fabrics associated with major thrusts precondition the rock to failure along both shallow- and deep-seated landslides (<100 m depth [*Dramis and Sorriso-Valvo*, 1994]) and the type of gravity-slide structures documented in the Sierra Nevada (<1.5 km depth [*Sanz de Galdeano and López-Garrido*, 1999]). Gravitational collapse of the type described in the Sierra Nevada is especially likely in regions where the normal faulting responsible for the formation of high relief is the same process that removes the rock buttresses at the margin of the mountain block.

[23] *Schmidt and Montgomery* [1995] argued that mountain relief might be strength limited, as rock strength mediates the depth and frequency of bedrock landslides. We argue that this concept may be extended to include deeper (>100 m) crustal processes such as tectonic denudation in general. This is consistent with the view that brittle upper crustal processes such as gravity sliding and bedrock landsliding contribute toward lateral extension and the gravitational collapse of mountain belts [*Avouac and Burov*, 1996; *Rey et al.*, 2001]. Our model of orogenic development is most applicable to either landscapes with low precipita-

tion or those incapable of supporting warm based glaciers in upland areas [cf. *Brozovic et al.*, 1997]. High-latitude glaciation may promote relief development through the opposing actions of cold and warm based glaciers; cold based glaciers can protect low-relief upland surfaces while warm based glaciers efficiently excavate deep U-shaped valleys [*Fabel et al.*, 2002; *Stroeven et al.*, 2002; *Li et al.*, 2005]. In warmer more humid regions, with a high drainage density, river incision may also provide an effective limit to relief [*Tucker and Slingerland*, 1997; *Tucker and Bras*, 1998; *Whipple et al.*, 1999; *Gabet et al.*, 2004]. Consequently, it seems likely that the behavior documented here will characterize small and hence relatively young active orogens in cold and/or arid to semiarid regions.

## 7. Conclusions

[24] Denudation of the Sierra Nevada has been accomplished through a range of processes from shallow bedrock landsliding to deeper gravity sliding within the crust. The upland areas of the western Sierra Nevada are insensitive to fluvial incision and surface processes are unable to keep pace with rapid rock uplift. Consequently, high-elevation areas maintain a low-relief landscape with low slope angles. However, at lower elevations close to the edge of the orogen, rivers and the adjacent hillslopes are sensitive to normal faulting at the mountain front and erosion rates are an order of magnitude faster than those in upland areas. This contrast in erosion rates dictates that overall relief of the mountain belt continues to increase until the limits of crustal strength are reached and gravity sliding occurs. Such deep-seated tectonic denudation provides an effective limit to relief with maximum relief controlled by the strength of the weakest rock mass or structure. The frequency and scale of movement of such detachments is controlled by normal faulting at the mountain front coupled to river incision at the edge of the mountain block. Such tectonic denudation, linked to rock uplift and inefficient fluvial incision near mountain tops seems likely to be episodic and may be a general characteristic of young orogens in cold and/or arid to semiarid regions.

## Appendix A: Interpretation of Cosmogenic Nuclide Concentrations in the Torrente Catchment

[25] The requirements for steady state erosion rate estimation from $^{10}$Be concentration in bedrock and fluvial sediment are discussed here. The $^{10}$Be concentration of quartz in fluvial sediments was assessed at three sites in the upper unrejuvenated catchment (MRS 3, MRS 12B, and MRS 18) and one in the lower rejuvenated catchment (MRS 21B). Erosion rates from fluvial sediment estimate the average erosion rate of all quartz-contributing areas [*Bierman and Steig*, 1996; *Granger et al.*, 1996]. Almost all of the quartz comes from the area to the east of the BMZ where quartz veins are ubiquitous and the weight% of quartz grains in each sediment sample is uniform (11 ± 2%); hence it is the average erosion rate of this area that we determine. The area west of the BMZ is dominated by metacarbonates of the Alpujárride complex, which contain negligible quartz. The dominant form of bedrock weathering in the upper catchment is downslope transport via slow diffusion of regolith that has been produced beneath a thin soil cover. The $^{10}$Be-based erosion rate estimates are unaffected by this type of regolith cover [*Granger et al.*, 1996].

[26] The $^{10}$Be technique requires that the rate of $^{10}$Be accumulation equals the rate of removal by erosion and radioactive decay [*Lal*, 1991]. Such a steady state is reached once ~3 m thickness of material is removed, under a regular weathering regime [*Bierman and Steig*, 1996; *Reinhardt et al.*, 2007]. In reality, most surfaces weather by detaching slabs, blocks or grains [cf. *Niemi et al.*, 2005]. This is especially true in the lower part of the Torrente catchment where rapid river incision and strong schistosity combine to promote shallow (<1 m) rock and debris slides. The $^{10}$Be concentration of regularly landsliding surfaces varies between being greater and less than the actual mean value, which is required for erosion rate estimation. Fortunately, this variability is minimal in regions where landslide depths do not exceed 1 m. *Reinhardt et al.* [2007] used finite difference approximations to quantify the variability in steady erosion rates due to bedrock spalling in the lower Torrente catchment and found that in situ and fluvial sediment-based erosion rates can be estimated by amalgamating an appropriate number of independent samples. Only one fluvial sediment sample (MRS 21B) was collected for $^{10}$Be analysis in the lower landside dominated catchment and the 56 g of pure quartz isolated for $^{10}$Be measurement probably contains enough grains ($>1 \times 10^6$) to represent all upstream erosional "events" <1 m depth [*Niemi et al.*, 2005; *Reinhardt et al.*, 2007]. In addition, the large volume of sediment in the lower catchment is primarily transported via infrequent debris flows. The $^{10}$Be measurements are not substantially affected by recent debris flow activity, as the time required for a typical sediment grain to be exhumed from a hillslope and transported to a small channel or hollow is much longer than the time required for it to be transported through the fluvial channel network [*Kirchner et al.*, 2001]. No large sedimentary deposits are observed upstream of the sampling sites.

[27] Prior to the establishment of the current climatic regime at circa 12 ka [*Jalut et al.*, 2000], the area was subject to periglacial (but not extensive glacial) activity [*Sánchez et al.*, 1990]. High-altitude areas must have been covered by snow during these and later times. However, we have chosen to ignore the shielding effect of snow cover on $^{10}$Be concentrations as this study focuses on order-of-magnitude variations in erosion rate unlikely to be affected by such considerations [*Schildgen et al.*, 2005]. During the postglacial transition to a relatively warm Holocene climate, erosion rates may have declined as periglacial activity became more restricted, potentially resulting in disequilibrium between nuclide concentrations in bedrock and sediment and the new erosion rates. Numerical analysis [*Riebe et al.*, 2001, Appendix 1, equations 5 and 6; *Reinhardt et al.*, 2007] indicates that this potential disequilibrium does not affect order-of-magnitude modern erosion

rates estimated from bedrock and fluvial sediments in the Torrente catchment provided that such rates have been regular during the Holocene.

[28] **Acknowledgments.** We gratefully acknowledge the support of the CRUST project (Scottish Higher Education Funding Council Research Development Grant), the Mac Robertson Travelling Scholarship (University of Glasgow), the Leverhulme and Carnegie trusts, and research grants from the Engineering and Physical Sciences Research Council and British Geomorphological Research Group. Anne Dunlop, Mike Shand, and Bill Higgison are thanked for their assistance with the digital photogrammetry cartography and geochemistry, and Tim Barrows and Keith Fifeld are thanked for their invaluable assistance with $^{10}$Be sample preparation and measurement at the ANU. We also thank Carlos Sanz de Galdeano for kindly giving us permission to reproduce his geological cross sections (Figure 6) and Zoe Shipton, Darrel Swift, and Rod Brown for helpful discussions during the preparation of this manuscript. University of Memphis contribution 506.

## References


Alfaro, P., J. Galindino-Zaldívar, A. Jabaloy, A. C. López-Garrido, and C. Sanz de Galdeano (1999), Evidencias de actividad y paleosismicidad de la falla de Padul (Cordillera Bética, sur de España), *Acta Geol. Hisp.*, *36*, 283–297.

Anhert, F. (1970), Functional relationships between denudation, relief and uplift in large mid-latitude drainage basins, *Am. J. Sci.*, *268*, 243–263.

Argles, T. W., J. P. Platt, and D. J. Waters (1999), Attenuation and excision of crustal section during extensional exhumation: The Carratraca Massif, Betic cordillera, southern Spain, *J. Geol. Soc. London*, *156*, 149–162.

Avouac, J. P., and E. B. Burov (1996), Erosion as a driving mechanism of intracontinental mountain growth, *J. Geophys. Res.*, *101*, 17,747–17,769.

Beck, A. (1968), Gravity faulting as a mechanism of topographic adjustment, *N. Z. J. Geol. Geophys.*, *11*, 191–199.

Bierman, P. R., and E. J. Steig (1996), Estimating rates of denudation using cosmogenic isotope abundances in sediment, *Earth Surf. Processes Landforms*, *21*, 125–139.

Bierman, P. R., M. C. Caffee, P. T. Davis, K. Marsella, M. Pavich, P. Colgan, D. Mickelson, and J. Larsen (2002), Rates and timing of Earth surface processes from in-situ-produced cosmogenic Be-10, in *Beryllium: Mineralogy, Petrology and Geochemistry*, *Rev. Mineral.*, vol. 50, edited by E. Grew, pp. 147–205, Mineral. Soc. of Am., Washington, D. C.

Braga, J. C., J. M. Martin, and C. Quesada (2003), Patterns and average rates of late Neogene-Recent uplift of the Betic Cordillera, SE Spain, *Geomorphology*, *50*, 3–26.

Brown, E., R. Stallard, M. Larsen, G. Raisbeck, and F. Yiou (1995), Denudation rates determined from the accumulation of in situ-produced $^{10}$Be in the Luquillo Experimental Forest, Puerto Rico, *Earth Planet. Sci. Lett.*, *129*, 193–202.

Brozovic, N., D. W. Burbank, and A. J. Meigs (1997), Climatic limits on landscape development in the northwestern Himalaya, *Science*, *276*, 571–574.

Burbank, D. W., J. Leland, E. Fielding, R. S. Anderson, N. Brozovic, M. R. Reid, and C. Duncan (1996), Bedrock incision, rock uplift and threshold hillslopes in the northwestern Himalayas, *Nature*, *379*, 505–510.

Calvache, M. L., C. Viseras, and J. Fernández (1997), Controls on fan development—Evidence from fan morphometry and sedimentology; Sierra Nevada, SE Spains, *Geomorphology*, *21*, 69–84.

Carrapa, B., J. Wijbrans, and G. Berotti (2003), Episodic denudation in the western Alps, *Geology*, *31*, 601–604.

Chamberlain, C. P., P. K. Zeitler, and E. Erickson (1991), Constraints on the tectonic evolution of the northwestern Himalaya from geochronologic and petrologic studies of Babusar Pass, Pakistan, *J. Geol.*, *99*, 829–849.

Codilean, A. T. (2006), Calculation of the cosmogenic isotope production topographic shielding scaling factor for large areas using DEM's, *Earth Surf. Processes Landforms*, *31*, 785–794.

Dempster, T. J., and C. Persano (2006), Low temperature thermochronology: Resolving geotherm shapes or denudation histories?, *Geology*, *34*, 73–76.

Dramis, F., and M. Sorriso-Valvo (1994), Deep seated slope deformations, related landslides and tectonics, *J. Eng. Geol.*, *38*, 231–243.

Dunkl, I. (2002), Tracckey: A windows program for calculation and graphical presentation of fission track data, *Comput. Geosci.*, *28*, 3–12.

Dunne, J., D. Elmore, and P. Muzikar (1999), Scaling factors for the rates of production of cosmogenic nuclides for geometric shielding and attenuation at depth on sloped surfaces, *Geomorphology*, *27*, 3–11.

Edwards, M. A., and T. M. Harrison (1997), When did the roof collapse? Late Miocene north-south extension in the high Himalaya revealed by Th-Pb monazite dating of the Khula Kangri granite, *Geology*, *25*, 543–546.

England, P., and P. Molnar (1990), Surface uplift, uplift of rocks and exhumation of rocks, *Geology*, *18*, 1173–1177.

Fabel, D., A. P. Stroeven, J. Harbor, J. Kleman, D. Elmore, and D. Fink (2002), Landscape preservation under Fennoscandian ice sheets determined from in situ produced $^{10}$Be and $^{26}$Al, *Earth Planet. Sci. Lett.*, *201*, 397–406.

Fernández, J., J. Soria, and C. Viseras (1996), Stratigraphic architecture of the Neogene basins in the central sector of the Betic cordillera (Spain): Tectonic control and base-level changes, in *Tertiary Basins of Spain: The Stratigraphic Record of Crustal Kinematics*, edited by P. F. Friend and C. J. Dabrio, pp. 353–365, Cambridge Univ. Press, New York.

Fifield, K. (1999), Accelerator mass spectrometry and its applications, *Rep. Prog. Phys.*, *62*, 1223–1274.

Gabet, E. J., B. A. Pratt-Situaula, and D. W. Burbank (2004), Climatic controls on hillslope angle and relief in the Himalayas, *Geology*, *32*, 629–632.

Galindino-Zaldívar, J., A. J. Gil, M. J. Borque, F. González-Lodiero, A. Jabaloy, C. Marín-Lechado, P. Ruano, and C. Sanz de Galdeano (2003), Active faulting in the internal zones of the central Betic Cordilleras (SE, Spain), *J. Geodyn.*, *36*, 239–250.

Gallagher, K. (1995), Evolving thermal histories from fission track data, *Earth Planet. Sci. Lett.*, *136*, 421–435.

García, A. F., Z. Zhu, T. L. Ku, C. Sanz de Galdeano, O. A. Chadwick, and J. Chacon Montero (2003), Tectonically driven landscape development within the eastern Alpujarran Corridor, Betic Cordillera, E Spain (Almería), *Geomorphology*, *50*, 83–110.

Garzione, C. N., P. G. DeCelles, D. G. Hodkinson, T. Ojha, and B. N. Upreti (2003), East-west extension and Miocene environmental change in the southern Tibetan plateau: Thakkhola graben, central Nepal, *Geol. Soc. Am. Bull*, *115*, 3–20.

Gleadow, A. J. W., and R. W. Brown (2000), Fission-track thermochronology and the long-term denudational response to tectonics, in *Geomorphology and Global Tectonics*, edited by M. A. Summerfield, pp. 57–75, John Wiley, Hoboken, N. J.

Gómez, A., D. Palacios, M. Ramos, L. M. Tanarro, L. Schulte, and F. Salvador (2001), Location of permafrost in marginal regions: Corral del Veleta, Sierra Nevada, Spain, *Permafrost Periglacial Processes*, *12*, 93–110.

Gómez-Ortiz, A., L. Schulte, and F. Salvador (1996), Contribucion al conocimiento de la deglaciacion reciente y morfologia asociada del Corral del Veleta (Sierra Nevada), *Cadernos Lab. Xeol. Laxe*, *21*, 543–558.

Gosse, J. C., and F. M. Phillips (2001), Terrestrial in situ cosmogenic nuclides: Theory and application, *Quat. Sci. Rev.*, *20*, 1475–1560.

Granger, D. E., and A. L. Smith (2000), Dating buried sediments using radioactive decay and muogenic production of $^{26}$Al and $^{10}$Be, *Nucl. Instrum. Methods Phys. Res., Sect. B*, *172*, 822–826.

Granger, D. E., J. W. Kirchner, and R. Finkel (1996), Spatially averaged long-term erosion rates measured from in situ produced cosmogenic nuclides in alluvial sediment, *J. Geol.*, *104*, 249–257.

Granger, D. E., C. Riebe, J. W. Kirchner, and R. C. Finkel (2001), Modulation of erosion on steep granitic slopes by boulder armouring, as revealed by cosmogenic $^{26}$Al and $^{10}$Be, *Earth Planet. Sci. Lett.*, *186*, 269–281.

Hodges, K. V., R. R. Parrish, T. B. Housh, D. R. Lux, B. C. Burchfiel, L. H. Royden, and Z. Chen (1992), Simultaneous Miocene extension and shortening in the Himalayan orogen, *Science*, *258*, 1466–1470.

Hovius, N., C. P. Stark, and P. A. Allen (1997), Sediment flux from a mountain belt derived by landslide mapping, *Geology*, *25*, 231–234.

Hovius, N., C. P. Stark, M. A. Tutton, and L. D. Abbott (1998), Landslide-driven drainage network evolution in a pre-steady-state mountain belt: Finisterre Mountains, Papua New Guinea, *Geology*, *26*, 1071–1074.

Hubbard, M. S., D. A. Spencer, and D. P. West (1995), Tectonic exhumation of the Nanga Parbat massif, northern Pakistan, *Earth Planet. Sci. Lett.*, *133*, 213–225.

Hughes, J. (1995), Studies in sedimentary provenance of the intramontane Granada Basin, southern Spain, Ph.D. thesis, Univ. of Glasgow, Glasgow, U. K.

Hurford, A. J., and P. F. Green (1982), A users' guide to fission track dating calibration, *Earth Planet. Sci. Lett.*, *59*, 343–354.

Hurford, A. J., M. Flisch, and E. Jäger (1989), Unravelling the thermo-tectonic evolution of the Alps: A contribution from fission track analysis and mica dating, in *Alpine Tectonics*, edited by M. P. Coward, D. Dietrich, and R. G. Park., *Geol. Soc. Spec. Publ.*, *45*, 369–398.

Jalut, G., A. A. Esteban, L. Bonnet, T. Gauquelina, and M. Fontugnec (2000), Holocene climatic changes in the western Mediterranean, from south-east France to south-east Spain, *Palaeogeogr. Palaeoclimatol. Palaeoecol.*, *160*, 255–290.

Johnson, C. (1994), Neogene tectonics in south eastern Spain: Constraints from fission track analysis, Ph.D. thesis, Univ. of London, London.

Johnson, C. (1997), Resolving denudational histories in orogenic belts with apatite fission-track thermochronology and structural data: An example from southern Spain, *Geology*, *25*, 623–626.

Johnson, C., N. Harbury, and A. J. Hurford (1997), The role of extension in the Miocene denudation of the Nevado-Filábride Complex, Betic Cordillera (SE Spain), *Tectonics*, *16*, 189–204.

Kapp, P., and J. H. Guynn (2004), Indian punch rifts Tibet, *Geology*, *32*, 993–996.

Keller, E. A., C. Sanz de Galdeano, and J. Chacón (1996), Tectonic geomorphology and earthquake hazard of Sierra Nevada southern Spain, in *1st Conferencia Internacional Sierra Nevada* (*Granada*), edited by J. Chacon and J. Rosua, pp. 201–218, Univ. of Granada-Sierra Nevada, Granada, Spain.

Kirchner, J. W., R. C. Finkel, C. S. Riebe, D. E. Granger, J. L. Clayton, J. G. King, and W. F. Megahan (2001), Mountain erosion over 10 yr, 10 K.y., and 10 M.y. time scales, *Geology*, *29*, 591–594.

Kohl, C., and K. Nishiizumi (1992), Chemical isolation of quartz for measurement of in-situ-produced cosmogenic nuclides, *Geochim. Cosmochim. Acta*, *56*, 3583–3587.

Kuhleman, J., W. Frisch, I. Dunkl, and B. Szekely (2001), Quantifying tectonic versus erosive denudation by the sediment budget: The Miocene core complexes of the Alps, *Tectonophysics*, *330*, 1–23.

Lal, D. (1991), Cosmic ray labelling of erosion surfaces: In situ nuclide production rates and erosion models, *Earth Planet. Sci. Lett.*, *104*, 424–439.

Lhénaff, R. (1997), Recherches Geomorphologiques sur les cor Dilleres Betiques Centre accidentales, PhD. thesis, Univ. de Lille 1, Villeneuve d'Ascq, France.

Li, Y., J. Harbor, A. P. Stroeven, D. Fabel, J. Kleman, D. Fink, M. Caffee, and D. Elmore (2005), Ice sheet erosion patterns in valley systems in northern Sweden investigated using cosmogenic nuclides, *Earth Surf. Processes Landforms*, *30*, 1039–1049.

Lonergan, L., and M. A. Mange-Rejetzky (1994), Evidence for Internal Zone unroofing from foreland basin sediments, Betic Cordillera, SE Spain, *J. Geol. Soc. London*, *151*, 515–529.

Martínez-Martínez, J. M., J. I. Soto, and J. C. Balanyá (2002), Orthogonal folding of extensional detachments: Structure and origin of the Sierra Nevada elongated dome (Betics, SE Spain), *Tectonics*, *21*(3), 1012, doi:10.1029/2001TC001283.

McClay, K. R., M. G. Nortan, P. Coney, and G. H. Davis (1986), Collapse of the Caledonian orogen and the old red sandstone, *Nature*, *323*, 147–149.

Mérnard, G., and P. Molnar (1988), Collapse of a Hercynian Tibetan Plateau into a late Palaeozoic European basin and range province, *Nature*, *334*, 235–237.

Niemi, N. A., M. Oskin, D. W. Burbank, A. J. Heimsath, and E. J. Gabet (2005), Effects of bedrock landslides on cosmogenically determined erosion rates, *Earth Planet. Sci. Lett.*, *237*, 480–498.

Platt, J. P., and J. H. Behrmann (1986), Structures and fabrics in a crustalscale shear zone, Betic Cordilleras, S.E. Spain, *J. Struct. Geol.*, *8*, 15–33.

Platt, J. P., and R. L. M. Vissers (1989), Extensional collapse of thickened continental lithosphere: A working hypothesis for the Alboran Sea and Gibraltar arc, *Geology*, *17*, 540–543.

Reinhardt, L. R. (2005), Tectonics and Topography: A study of mountain denudation in southern Spain, Ph.D. thesis, 164 pp., Univ. of Glasgow, Glasgow, U. K., 2 July .

Reinhardt, L. R., T. B. Hoey, T. T. Barrows, T. J. Dempster, P. Bishop, and L. K. Fifield (2007), Interpreting erosion rates from cosmogenic radionuclide concentrations measured in rapidly eroding terrain, *Earth Surf. Processes Landforms*, doi:10.1002/esp.1415, in press.

Rey, P., O. Vanderhaeghe, and C. Teyssier (2001), Gravitational collapse of the continental crust: Definition, regimes and modes, *Tectonophysics*, *342*, 435–449.

Riebe, C., J. W. Kirchner, D. E. Granger, and R. C. Finkel (2001), Minimal climatic control on erosion rates in the Sierra Nevada, California, *Geology*, *29*, 447–450.

Ring, U., M. T. Brandon, S. D. Willett, and G. S. Lister (1999), *Exhumation Processes: Normal Faulting, Ductile Flow and Erosion*, *Geol. Soc. Spec. Publ.*, *154*.

Rodríguez-Fernández, J., C. Sanz de Galdeano, and J. Fernández (1989), Genesis and evolution of the Granada Basin (Betic Cordillera, Spain), in *International Symposium on Intermontane Basins: Geology and Resources*, edited by T. Thauasuthipitak, and P. Ounchanum, pp. 294–305, Chiang Mai, Thailand.

Roering, J. J., J. W. Kirchner, and W. E. Dietrich (2005), Characterizing structural and lithologic controls on deepseated landsliding: Implications for topographic relief and landscape evolution in the Oregon Coast Range, USA, *Geol. Soc. Am. Bull.*, *117*, 654–668.

Sánchez, S., M. Simón, and I. García (1990), Morfogensis glaciar de la cuenca del Ñacute;o Lanjaron (Sierra NevadaGranada), in *Actas 1 Reunión Nacional de Geomorfología*, edited by M. Gutiérrez, J. Peña, and M. Lozano, pp. 203–210, Soc. Esp. de Geomorfol., Teruel, Spain.

Sánchez-Marañón, M., R. Delgada, J. Párraga, and G. Delgada (1996), Multivariate analysis in the quantitative evaluation of soils for reforestation in the Sierra Nevada (southern Spain), *Geoderma*, *69*, 233–248.

Sanz de Galdeano, C. (1996), Neotectonica y nectonica activa en el sector de Padul-Durcal (borde sw de Sierra Nevada, Espańa), in *1st Conferencia Internacional Sierra Nevada*, vol. 1, edited by J. Chacon and J. Rosua, pp. 219–231, Univ. of Granada-Sierra Nevada, Granada, Spain.

Sanz de Galdeano, C., and A. C. López-Garrido (1999), Nature and impact of the neotectonic deformation in the western Sierra Nevada (Spain), *Geomorphology*, *30*, 259–272.

Savage, W. Z., and D. J. Varnes (1987), Mechanics of gravitational spreading of steepsided ridges ('sackung'), *Bull. Int. Assoc. Eng. Geol.*, *35*, 31–36.

Schildgen, T. F., W. M. Phillips, and R. S. Purves (2005), Simulation of snow shielding corrections for cosmogenic nuclide surface exposure studies, *Geomorphology*, *64*, 67–85.

Schmidt, K. M., and D. R. Montgomery (1995), Limits to relief, *Science*, *270*, 617–620.

Shroder, J. F., Jr. (1998), Slope failure and denudation in the western Himalaya, *Geomorphology.*, *26*, 81–105.

Shroder, J. F., Jr., and M. Bishop (1998), Mass movement in the Himalaya: New insights and research directions, *Geomorphology*, *26*, 13–35.

Simón, M., S. Sanchez, and I. Garcia (2000), Soillandscape evolution on a Mediterranean high mountain, *Catena*, *39*, 211–231.

Small, E. E., R. S. Anderson, J. L. Repka, and B. R. Finkel (1997), Erosion rates of alpine bedrock summit surfaces deduced from in situ $^{10}$Be and $^{26}$Al, *Earth Planet. Sci. Lett.*, *150*, 413–425.

Sorkhabi, R. B., E. Stump, K. A. Foland, and A. K. Jain (1996), Fission track and $^{40}$Ar/$^{39}$Ar evidence for episodic denudation of the Gangotri granites in the Garhwal higher Himalaya, India, *Tectonophysics*, *260*, 187–189.

Stone, J. O. (2000), Air pressure and cosmogenic isotope production, *J. Geophys. Res.*, *105*, 23,753–23,759.

Stroeven, A. P., D. Fabel, C. Hättestrand, and J. Harbor (2002), A relict landscape in the centre of Fennoscandian glaciation: Cosmogenic radionuclide evidence of tors preserved through multiple glacial cycles, *Geomorphology*, *44*, 145–154.

Tucker, G. E., and R. L. Bras (1998), Hillslope processes, drainage density, and landscape morphology, *Water Resour. Res.*, *34*, 2751–2764.

Tucker, G. E., and R. Slingerland (1997), Drainage basin response to climate change, *Water Resour. Res.*, *33*, 2031–2047.

Van Bemmelen, R. W. (1954), *Mountain Building*, Martinus Nijhoff, Zoetermeer, Netherlands.

Vance, D., M. Bickle, S. Ivy-Ochs, and P. Kubik (2003), Erosion and exhumation in the Himalaya from cosmogenic isotope inventories of river sediments, *Earth Planet. Sci. Lett.*, *206*, 273–288.

Whipple, K. X., and G. E. Tucker (1999), Dynamics of the streampower river incision model: Implications for height limits of mountain ranges, landscape response timescales, and research needs, *J. Geophys. Res.*, *104*, 17,661–17,674.

Whipple, K. X., E. Kirby, and S. H. Brocklehurst (1999), Geomorphic limits to climateinduced increases in topographic relief, *Nature*, *40*, 39–43.

T. J. Dempster and C. Persano, Department of Geographical and Earth Sciences, University of Glasgow G12 8QQ, Glasgow, UK.

L. J. Reinhardt, Center for Earthquake Research and Information, University of Memphis, 3876 Central Avenue, Memphis, TN 38152, USA. (wjrnhrdt@memphis.edu)

J. F. Shroder Jr., Department of Geography and Geology, University of Nebraska at Omaha, Omaha, NE 68182, USA.